The Instabilities and Multiscale Energetics Underlying the Mean–Interannual–Eddy Interactions in the Kuroshio Extension Region

YANG YANG

School of Atmospheric Sciences, Nanjing University of Information Science and Technology, Nanjing, China

X. SAN LIANG

School of Marine Sciences, and School of Atmospheric Sciences, Nanjing University of Information Science and Technology, Nanjing, China

ABSTRACT

Using a recently developed energetics diagnostic methodology, namely, the localized multiscale energy and vorticity analysis (MS-EVA), this study investigates the intricate nonlinear mutual interactions among the decadally modulating mean flow, the interannual fluctuations, and the transient eddies in the Kuroshio Extension region. It is found that the mean kinetic energy maximizes immediately east of the Izu–Ogasawara Ridge, while the transient eddy kinetic energy does not peak until 400 km away downstream. The interannual variabilities, which are dominated by a jet-trapped Rossby wave mode, provide an energy reservoir comparable to the other counterparts. In the upstream, strong localized barotropic and baroclinic transfers from the mean flow to the eddies are observed, whereas those from the interannual variabilities are not significant. Besides fueling the eddies, the unstable mean jet also releases energy to the interannual-scale processes. Between 144° and 154°E, both transfers from the mean flow and the interannual variabilities are important for the eddy development. Farther downstream, eddies are found to drive the mean flow on both the kinetic energy (KE) and available potential energy (APE) maps. They also provide KE to the interannual variabilities but obtain APE from the latter. The gained eddy APE is then converted to eddy KE through buoyancy conversion. Upscale energy transfers are observed in the northern and southern recirculation gyre (RG) regions. In these regions, the interannual–eddy interaction exhibits different scenarios: the eddies lose KE to the interannual processes in the northern RG region, while gaining KE in the southern RG region.

1. Introduction

As one of the major western boundary currents (WBCs), the Kuroshio carries momentum and heat northward from the tropics to midlatitude regions. After leaving from Japan, it flows zonally into the North Pacific Ocean. This zonal jet is called Kuroshio Extension (see Fig. 1). The Kuroshio Extension acts as a frontal boundary of abrupt change in temperature and salinity. Large-amplitude stationary meanders and vigorous mesoscale eddies have been observed by satellite altimeters (e.g., Tai and White 1990; Qiu et al. 1991; Ebuchi and Hanawa 2001; Nakamura and Kazmin 2003; Itoh and Yasuda 2010; Greatbatch et al. 2010),

hydrographic observations (e.g., Bernstein and White 1981; Mizuno and White 1983; Joyce 1987; Jayne et al. 2009; Tracey et al. 2012), as well as confirmed by a number of numerical studies (e.g., Tai and Niiler 1985; Hurlburt et al. 1996; McCalpin and Haidvogel 1996; Kelly et al. 2007; Aoki et al. 2013).

The Kuroshio Extension exhibits a broadband of temporal variabilities. In addition to intense eddy variabilities with temporal scales varying from weeks to months (Tai and White 1990; Qiu 1995; Ebuchi and Hanawa 2000; Itoh and Yasuda 2010), the system also reveals significant interannual fluctuations (Mizuno and White 1983; Yamagata et al. 1985; Adamec 1998; Qiu 2000) and a well-defined decadal modulation (Qiu and Chen 2005; Sasaki et al. 2013). These multiscale oceanic systems have a great impact on the cross-stream exchange of mass and tracers, and they may influence each other through complex-scale interactions. For

Corresponding author address: X. San Liang, Nanjing Institute of Meteorology, 219 Ningliu Blvd., Nanjing 210044, China.
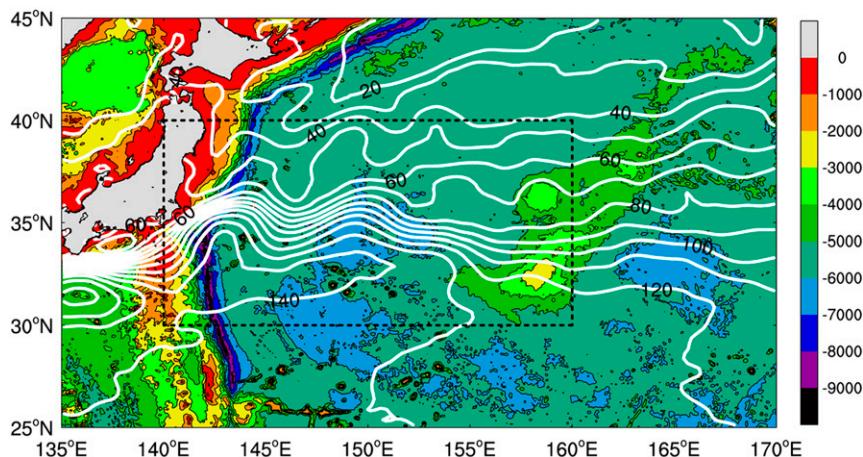E-mail: sanliang@courant.nyu.edu

FIG. 1. Mean dynamic topography (white contours; cm) based on the Archiving, Validation, and Interpretation of Satellite Oceanographic (AVISO) data and bathymetry (colored; m). The region enclosed by dashed lines is the research domain of this study.

instance, Penduff et al. (2011) suggested that the interannual variability appears to be prominent in ocean sectors where mesoscale eddies are active, implying that a portion of low-frequency variability is introduced by mesoscale eddies through nonlinear-scale interactions.

The Kuroshio Extension has been observed as one of the highest mesoscale eddy kinetic energy (EKE) regions in the global ocean (Wyrtki et al. 1976; Ferrari and Wunsch 2009). In the presence of strong shear of the eastward-flowing jet, eddies extract energy from the mean flow through baroclinic and barotropic instabilities (Williams et al. 2007; Spall 2000; von Storch et al. 2012; Bishop 2013). Although the intensity of the eddy variability in the Kuroshio Extension may be related to the status of background mean flow, the response of mesoscale eddies to the mean flow is not necessarily passive. Qiu and Chen (2010) reported that the enhanced eddy variability acts to strengthen the southern recirculation gyre (SRG). By analyzing an eddy-resolving multidecadal hindcast simulation, Taguchi et al. (2010) suggested that the eddy feedback may contribute to the low-frequency modulation of the northern recirculation gyre (NRG) intensity at middepth. Recently, Delman et al. (2015) indicated that eddies along the jet tend to reinforce the quasi-permanent meanders and drive its flanking recirculation gyres. Other theoretical and observational studies also emphasized the importance of upscale feedback from mesoscale eddies to the large-scale currents, which oscillate on interannual to decadal time scales (Spall 1996; Penduff et al. 2011; Arbic et al. 2014).

Previous studies have suggested that processes in the Kuroshio Extension region tend to occur on a range of scales or scale windows, as introduced by Liang and Robinson (2004) and Liang and Anderson (2007).

Specifically, there is a decadally modulating window, an interannually fluctuating window, and a transient eddy window. Numerous studies emphasized the importance of a two-way interaction between the mean flow and the eddies. However, using diagnostic tools that partition a field into a mean and an eddy part only is difficult to distinguish between the relative contributions from three or more than three windows. In other words, it is hard to unravel the decadal–interannual–eddy interactions. The approach of Reynolds mean–eddy decomposition based on time averaging, a technique widely used in previous energetics studies, will leave low-frequency variability in the transient eddy window; those relying on a conventional temporal high-pass filter to define eddies essentially cannot have a faithful representation of the multiscale processes due to the failure to conserve energy (Liang and Anderson 2007). Up to now, it is still unclear how the magnitude and sign of the energy transfer from the mean flow to the eddies in the Kuroshio Extension region may vary in space and time. Also unclear is the relative contribution from the eddy–mean flow interaction and eddy–interannual interaction to the eddy growth/decay in this region. These issues, among others, motivate us to investigate the Kuroshio Extension from a multiscale point of view.

Multiscale interactions are ubiquitous in real oceans, and they are in nature highly nonlinear and intermittent in space and time. Multiscale energetics are natural measures of the interactions. They are closely tied to hydrostability, an important geophysical fluid dynamics (GFD) process, which belongs to a kind of energy transfer between scale windows. Using a new functional analysis tool by Liang and Anderson (2007), the multiscale window transform (MWT), Liang and Robinson

(2005, 2007) developed a methodology, namely, the localized multiscale energy and vorticity analysis (MS-EVA) for the diagnosis of those energetics. They proved that a unique energy transfer expression can be achieved locally, allowing for a faithful representation of the local interactions between various scales. This methodology is rigorous in mathematics and physics and has been applied successfully to different ocean problems (Liang and Robinson 2004, 2009; Xie et al. 2007). A more detailed introduction of the MS-EVA will be provided in section 2.

Using MS-EVA, in this study we will separate the associated fields into three parts: the decadally modulating mean flow, the interannual fluctuation, and the transient eddies, each within a scale window, and estimate how the three windows interact with each other in the Kuroshio Extension region. The rest of the paper is organized as follows: We briefly introduce the MS-EVA in section 2 and the OFES data description in section 3. The MS-EVA analysis is set up in section 4, and the major results are shown in sections 5–6. Section 7 summarizes this study.

2. A brief review of the localized energy and vorticity analysis

Multiscale energetics analysis provides quantitative information of intrinsic and external energy sources and sinks in the form of multiscale energy budget equations. The research methodology for this study is MS-EVA (Liang and Robinson 2005); also to be used is the MS-EVA-based theory of localized, finite-amplitude baroclinic and barotropic instabilities (Liang and Robinson 2007), which are given a brief review herein. Consider the Navier–Stokes equations with hydrostatic and Boussinesq approximations:

$$\frac{\partial u}{\partial t} = -\nabla \cdot (u\mathbf{u}) + fv - \frac{1}{\rho_0}\frac{\partial p}{\partial x} + F_u, \tag{1}$$

$$\frac{\partial v}{\partial t} = -\nabla \cdot (v\mathbf{u}) - fu - \frac{1}{\rho_0}\frac{\partial p}{\partial y} + F_v, \tag{2}$$

$$0 = \nabla \cdot \mathbf{u}, \tag{3}$$

$$0 = -\frac{\partial p}{\partial z} - \rho g, \quad \text{and} \tag{4}$$

$$\frac{\partial \rho}{\partial t} = -\nabla \cdot (\rho\mathbf{u}) - \frac{\rho_0 N^2}{g} w + F_\rho, \tag{5}$$

where $\mathbf{u} = (u, v, w)$ is the velocity vector, $\nabla\cdot$ is the three-dimensional divergence operator, F is the external forcing/dissipation, and others are conventional. Here, ρ is the density perturbation from the background profile $\bar{\rho}(z)$, and p is the dynamic pressure related to ρ.

The MS-EVA is based on a new functional analysis tool, multiscale window transform, introduced by Liang and Anderson (2007). With the MWT, one can split a function space into a direct sum of several mutually orthogonal subspaces, each with an exclusive range of time scales. Such a subspace is termed a scale window. One may have as many scale windows as one likes; for this study, we select three, namely, a decadal-scale mean flow window, an interannual-scale window, and an eddy window. For easy reference, they are denoted by $\varpi = 0$, 1, and 2, respectively.

For a given time series $[S(t)]$, application of the MWT yields the MWT coefficient $\hat{S}_n^{\sim\varpi}$ [$(\hat{\cdot})_n^{\sim\varpi}$ denotes MWT on window ϖ at time step n]. The MWT has many nice properties, one being the property of marginalization, which allows for a precise representation of multiscale energy as the product of the MWT coefficients, up to a constant. For example, the energy of S on window ϖ at time step n E_n^ϖ is proportional to $(\hat{S}_n^{\sim\varpi})^2$. It is further proved that, for a scalar field S within a flow $\mathbf{u}$, the energy transfer from other scale windows to the window ϖ is

$$T_n^\varpi = -E_n^\varpi \nabla \cdot \mathbf{u}_S^\varpi, \tag{6}$$

where

$$\mathbf{u}_S^\varpi = \frac{\widehat{(\mathbf{u}S)}_n^{\sim\varpi}}{\hat{S}_n^{\sim\varpi}} \tag{7}$$

is referred to as the S-coupled velocity. This transfer expression has an interesting property, namely,

$$\sum_\varpi \sum_n T_n^\varpi = 0, \tag{8}$$

as proved in Liang and Robinson (2005, 2007) and Liang and Anderson (2007). Equation (8) works for decompositions with arbitrary many windows; particularly, it works for a two-window decomposition. Note that the two-window MS-EVA is different from the traditional mean–eddy decomposed energetics formalism (e.g., Brooks and Niiler 1977). The energy transfer terms in the traditional mean and eddy energy equations sum to a divergence form, which is in general not zero. This is not what one would expect, as physically a transfer process should merely redistribute energy among scales, without generating or destroying energy as a whole. To distinguish, this process in the MS-EVA formalism T_n^ϖ is termed "canonical transfer."

Within the MWT framework, the kinetic energy (KE) and available potential energy (APE) density on window ϖ at time step n can be defined as follows:

$$K_n^\varpi = \frac{1}{2}\rho_0 \hat{\mathbf{u}}_n^{\sim\varpi} \cdot \hat{\mathbf{u}}_n^{\sim\varpi}, \quad \text{and} \qquad (9)$$

$$A_n^\varpi = \frac{1}{2}c(\hat{\rho}_n^{\sim\varpi})^2, \qquad (10)$$

respectively. The coefficient $c = g^2/(\rho_0 N^2)$ is introduced for conciseness. This definition is the same as the classical one (e.g., Gill 1982). The two types of energy densities within the MWT framework are conserved, which is not met in previous formalisms using the conventional filters. With a careful separation of intertwined nonlinear processes into a transport and a canonical transfer, Liang and Robinson (2005) obtained

$$\frac{\partial K_n^\varpi}{\partial t} + \underbrace{\nabla \cdot \left[\frac{1}{2}\rho_0 \hat{\mathbf{u}}_n^{\sim\varpi} \widehat{(\mathbf{u}\mathbf{u}_H)}_n^{\sim\varpi} \right]}_{\Delta Q_{K,n}^\varpi} + \underbrace{\nabla \cdot (\hat{\mathbf{u}}_n^{\sim\varpi} \hat{p}_n^{\sim\varpi})}_{\Delta Q_{P,n}^\varpi}$$

$$= \underbrace{-\left[\frac{1}{2}\rho_0 (\hat{u}_n^{\sim\varpi})^2 \nabla \cdot \mathbf{u}_u^\varpi + \frac{1}{2}\rho_0 (\hat{v}_n^{\sim\varpi})^2 \nabla \cdot \mathbf{u}_v^\varpi \right]}_{T_{K,n}^\varpi}$$

$$+ \underbrace{(-g\hat{\rho}_n^{\sim\varpi} \hat{w}_n^{\sim\varpi})}_{b_n^\varpi} + F_{K,n}^\varpi, \quad \text{and} \qquad (11)$$

$$\frac{\partial A_n^\varpi}{\partial t} + \underbrace{\nabla \cdot \left[\frac{1}{2}c\hat{\rho}_n^{\sim\varpi} \widehat{(\rho\mathbf{u})}_n^{\sim\varpi} \right]}_{\Delta Q_{A,n}^\varpi}$$

$$= \underbrace{-A_n^\varpi \nabla \cdot \mathbf{u}_\rho^\varpi}_{T_{A,n}^\varpi} + \underbrace{g\hat{\rho}_n^{\sim\varpi} \hat{w}_n^{\sim\varpi}}_{-b_n^\varpi} + F_{A,n}^\varpi, \qquad (12)$$

where $\mathbf{u}_H$ is the horizontal velocity vector, and the coupled velocities in Eqs. (11) and (12) satisfy Eq. (7) for $S = u$, v, or ρ. Note the ΔQ and T terms are very different from those in classical formalisms. One can see in the MWT framework, the multiscale energy equations can be written in a more concise form, that is, the mean kinetic energy (MKE, K_n^0), interannual-scale kinetic energy (IKE, K_n^1), and EKE (K_n^2) equations can be merged into one universal form as Eq. (11); similarly, the mean available potential energy (MAPE, A_n^0), interannual-scale available potential energy (IAPE, A_n^1), and eddy available potential energy (EAPE, A_n^2) equations are integrated to Eq. (12). Within Eqs. (11) and (12), the ΔQ terms represent the nonlocal process of energy flux divergence through advection $\Delta Q_{K,n}^\varpi$ or pressure work $\Delta Q_{P,n}^\varpi$. The b terms are the rate of buoyancy conversion between the APE and KE. The T terms, that is, the canonical transfers, represent the local process of energy transfer due to interwindow interactions. The forcing and dissipation processes (the F terms) are not explicitly expressed here, since they are not considered in this

study. Summing the T terms over all the possible windows and sampled time gives the property shown in Eq. (8). This is one of the major differences between the MS-EVA formalism and the classical ones.

In Eqs. (11) and (12), the transfer terms are $T_{K,n}^\varpi$ and $T_{A,n}^\varpi$. It has been established that after applying a technique-named interaction analysis, they will correspond precisely to the two important geophysical fluid flow processes, that is, the barotropic instability and baroclinic instability (Liang and Robinson 2007). That is to say, these transfer terms can be further decomposed to unravel the complicated window–window interactions. For example, the transfer function in the eddy window ($\varpi = 2$) from kinetic energy equation can be cast into the following four groups: $T_{K,n}^{0\rightarrow 2}$, $T_{K,n}^{1\rightarrow 2}$, $T_{K,n}^{0\oplus 1\rightarrow 2}$, and $T_{K,n}^{2\rightarrow 2}$ [for details, see Liang and Robinson (2005)]. Specifically, $T_{K,n}^{0\rightarrow 2}$ and $T_{K,n}^{1\rightarrow 2}$ are transfer rates from the mean flow window ($\varpi = 0$) and interannual-scale window ($\varpi = 1$); $T_{K,n}^{0\oplus 1\rightarrow 2}$ is the combined contribution from the window 0 and window 1 interaction. The last term $T_{K,n}^{2\rightarrow 2}$ represents the part of transfer from the same window between different time steps. Since terms like $T_{K,n}^{0\oplus 1\rightarrow 2}$ are generally much smaller compared to other terms, and we are not concerned about transfer from the same window between different time steps (they are irrelevant to stability/instability), we will particularly focus on the energy transfer across two different windows. These window–window terms are essentially the two critical quantities that measure the two instabilities, namely, barotropic and baroclinic transfers. For instance, in a three-window decomposition, we have three barotropic transfer fields, $T_{K,n}^{0\rightarrow 1}$, $T_{K,n}^{0\rightarrow 2}$, and $T_{K,n}^{1\rightarrow 2}$, as indicators for barotropic instability. Positive (negative) values of $T_{K,n}^{0\rightarrow 1}$, $T_{K,n}^{0\rightarrow 2}$, and $T_{K,n}^{1\rightarrow 2}$ imply mean-to-interannual (interannual to mean), mean-to-eddy (eddy to mean), and interannual-to-eddy (eddy to interannual) energy transfers. These terms are essential to examine the multiscale interactions due to barotropic instability. There are three additional terms like $T_{K,n}^{1\rightarrow 0}$, $T_{K,n}^{2\rightarrow 0}$, and $T_{K,n}^{2\rightarrow 1}$ in MS-EVA kinetic energy formulation. These terms are the opposite field of $T_{K,n}^{0\rightarrow 1}$, $T_{K,n}^{0\rightarrow 2}$, and $T_{K,n}^{1\rightarrow 2}$, depending on in which window one stands to interpret them. Positive (negative) values of $T_{K,n}^{1\rightarrow 0}$, $T_{K,n}^{2\rightarrow 0}$, and $T_{K,n}^{2\rightarrow 1}$ imply interannual-to-mean (mean to interannual), eddy-to-mean (mean to eddy), and eddy-to-interannual (interannual to eddy) energy transfers. It will be shown that these terms are generally the opposite sign to that of $T_{K,n}^{0\rightarrow 1}$, $T_{K,n}^{0\rightarrow 2}$, and $T_{K,n}^{1\rightarrow 2}$ in the Kuroshio Extension region.

Notice that many previous studies used the buoyancy conversion, that is, b_n^ϖ in this study, as the indicator for baroclinic instability. We remark that the two are different concepts. Classically, baroclinic instability is defined as the perturbation energy growth due to baroclinicity; an
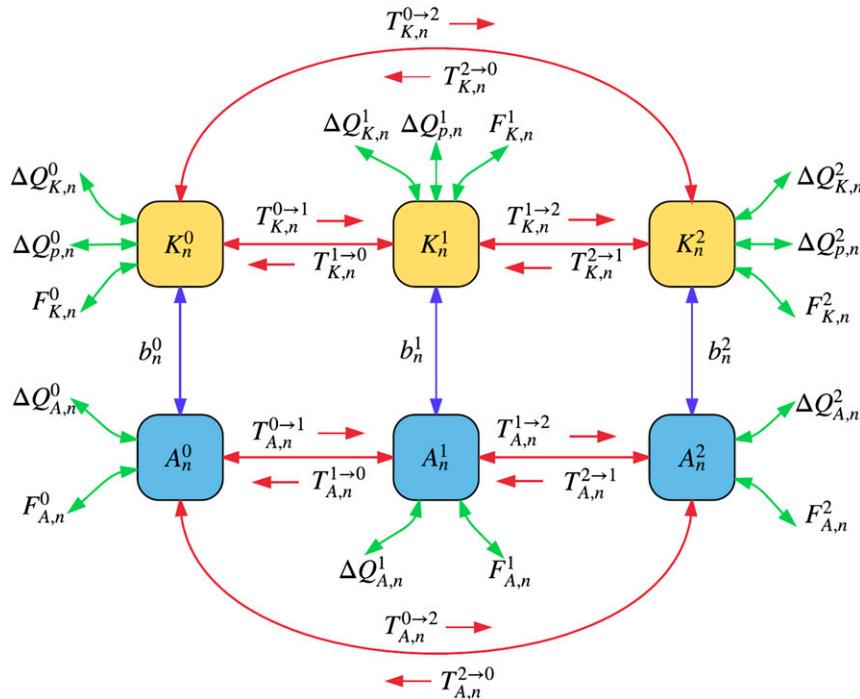
FIG. 2. A schematic of the multiscale energy pathway for a three-window decomposition. Red arrows indicate the energy transfers within different scale windows, while blue arrows illustrate the buoyancy conversion connecting the KE and APE reservoirs. The symbols are the same as those in Eqs. (11) and (12). Interaction analyses are indicated in the superscripts of the T terms. For clarity, transfers within the same window and transfers from two windows to the other are not shown.

explicit mathematical expression can be found in Pedlosky (1987). It is a bulk concept averaged over space with localized structure eliminated. However, atmospheric and oceanic processes are generally inhomogeneous; they usually have a spatial structure. Realizing the gap between the theory and reality, people have sought surrogates for the identification of baroclinic instability, and buoyancy conversion is the most popular one. It is a field variable and so has all the localized information retained. This surrogate, which has a clear physical meaning of conversion from perturbation potential energy to kinetic energy, indeed has been successfully used for baroclinic instability identification in many applications. However, buoyancy conversion is by no means equivalent to baroclinic instability. They are different concepts, anyway, and the difference has been shown in many examples with both classical idealized models (e.g., Liang and Robinson 2007) and realistic ocean problems (e.g., Liang and Robinson 2004). On the other hand, the barotropic instability and baroclinic instability in the MS-EVA framework are rigorously derived in the classical sense with localized information retained. See Liang and Robinson (2007) for detailed derivation.

By collecting the MS-EVA terms, we can classify the energetic processes into four categories: energy transport (flux divergence), canonical transfer, buoyancy conversion, and dissipation/diffusion. The divergence of energy fluxes vanishes if integrated over a closed domain; buoyancy conversion connects KE and APE on each individual window, while canonical transfer acts to redistribute energy between different scale windows. To summarize, Fig. 2 shows the energy diagram based on a three-window decomposition. In this study, we will only focus on the energy transfer (red arrows) and buoyancy conversion (blue arrows) processes, since they are essential to discern the intrinsic multiscale interactions of the Kuroshio Extension system.

3. Data description

One of the difficulties in performing analysis of the multiscale energetics of the in situ observations is that the observed records are too short. Besides, the information obtained by satellites is merely limited to the sea surface. Fortunately, the multidecadal hindcast of the OGCM for the Earth Simulator (OFES) provides an opportunity to overcome the above obstacles. The OFES dataset has been widely used for examining the decadal variability as well as the eddy statistics of the Kuroshio Extension recently and compared noticeably

well with the satellite sea surface height (SSH) observations (Nonaka et al. 2006, 2008, 2012; Taguchi et al. 2007, 2010; Sasaki and Schneider 2011). We use the output of OFES to fulfill this study. Here, the model configuration is briefly described; details are referred to Masumoto et al. (2004) and Sasaki et al. (2008). The OFES is based on the Modular Ocean Model, version 3 (MOM3; Pacanowski and Griffies 1999), which is a 3D, z-level, hydrostatic, Boussinesq ocean model, extending from 75°S to 75°N with a 0.1° horizontal resolution. Vertically, the model has 54 levels, with resolution varying from 5 m near the sea surface to 330 m near the bottom at a maximum depth of 6065 m. After a 50-yr spinup started with annual-mean fields of temperature and salinity of the *World Ocean Atlas 1998* (*WOA98*) with no motion and driven by monthly climatological forcing from the NCEP–NCAR reanalysis data, the OFES hindcast simulation is driven with the daily mean NCEP–NCAR reanalysis data from 1950 to 2011. The 3-day outputs from 1980 to 2011 are used for this study.

4. MS-EVA setup

The first step to set up an MS-EVA application is to determine the cutoff periods of the scale window decomposition. In this study, we need two cutoff periods to separate the dynamics into three scale windows. The power spectrum analysis is utilized to define the dominant spectrum peaks of the SSH field for a sequence of grid points selected in our study domain (not shown). In general, the spectra are dominated by a decadal period around 10 yr, the annual cycle, and a broadband of peaks corresponding to time scales shorter than 3 months that are considered to indicate transient eddy variabilities in this area. Using the SSH anomaly data derived from the TOPEX/Poseidon altimeter, Itoh and Yasuda (2010) determined the major periods of mesoscale eddies in the Kuroshio–Oyashio Extension region to be 4–12 weeks. They also found that the long-lived eddies with life cycles longer than 12 weeks and shorter than 52 weeks still contribute a large portion to the total SSH variance in this area. Based on this and what we have learned from the spectrum analysis, we set the cutoff periods to be 8 and 1 yr, respectively. That is to say, processes with periods longer than 8 yr are defined as the mean flow in this study, those with periods between 1 and 8 yr are treated as the interannual fluctuations, and the remaining high-pass signals represent the eddy activities. We have tested the second cutoff period from 6 months to 2 yr, and the results are quantitatively similar. Figure 3 depicts the raw data and three reconstructed components of the SSH field on two typical days from the simulation. Clearly, the mean feature has a time dependence, that is,

it is nonstationary (Figs. 3c,d). In this sense, previous studies using time average as the mean flow work only if the system is stationary; besides, if a decomposition is achieved by a time averaging, the transient eddy window will include the low-frequency variability, resulting in unconvincing scale interaction results. The interannual fluctuation field depicts a wave train–like pattern, which seems to be mostly confined along the mean jet (Figs. 3e,f). Lin et al. (2014) used a frequency-dependent Hilbert empirical orthogonal function analysis to show that the interannual mode of the observed sea level variability in the Kuroshio Extension region could be explained as a jet-trapped Rossby wave. The transient eddy field is defined as periods shorter than 1 yr in this study (see Figs. 3g,h). Both the shape and duration of the eddies resemble the eddy characteristics from previous studies in this region. They are generally propagating westward and interact with the mean jet intermittently.

5. Multiscale energy

Before investigating the energy transfers and buoyancy conversions, we first examine the spatial structures of the multiscale energy components averaged over the entire hindcast period. The first and last years are excluded just in case the boundary effect might arise. Figure 4 exhibits the horizontal and longitudinal distribution of the vertically averaged KE components. The longitudinal fields are meridionally averaged between 34° and 36°N, which bound the jet path. The time-mean MKE describes the strong zonal jet (Fig. 4a), which is significantly steered by the bottom topography of the Izu–Ogasawara Ridge. The contours of the meridional velocity are added in Fig. 4a to show the two quasi-stationary meanders that form downstream from the topography, with their mean crests located around 143°–144° and 150°E, respectively. The distance between the two crests is expected by the wavelength calculated by the stationary Rossby lee-wave dispersion relation, consistent with the observation (Mizuno and White 1983). The longitudinal distribution of MKE shows that the MKE maximizes immediately downstream from the topography and then decays dramatically as the jet flows eastward (Fig. 4b). Unlike MKE, the transient EKE does not peak until ~400 km downstream of the topography (Fig. 4e); it remains significantly high along the jet path from 144° to 154°E and then decays rapidly further to the downstream regions (Fig. 4f). This localized feature of the anomalously high EKE is also found in previous studies using satellite altimeters (Qiu and Chen 2010) and numerical simulations (Kelly et al. 2007). Similar to EKE, the IKE reservoir is characterized by a strong maximum center near 144°–145°E and then gradually decreases to
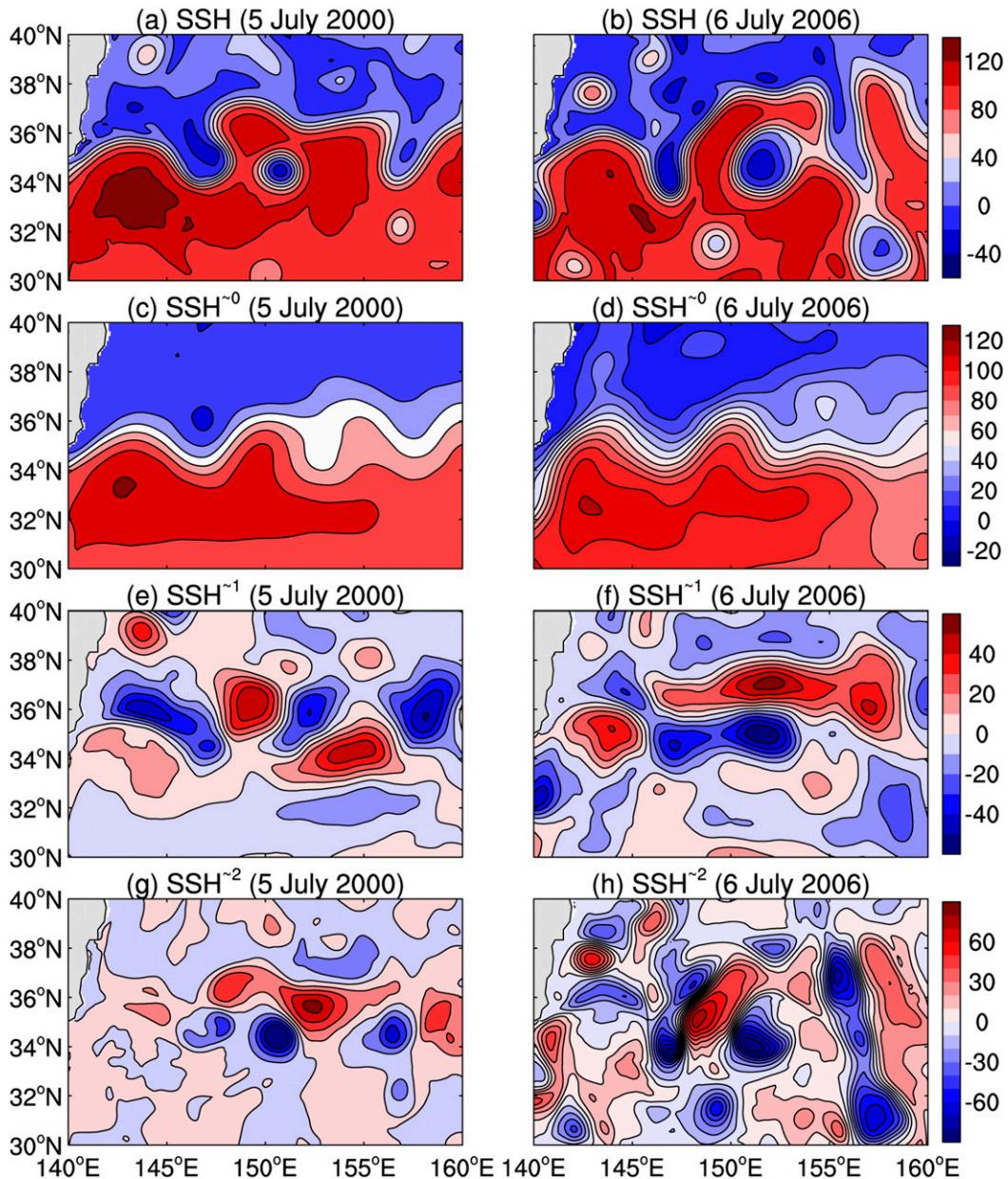
FIG. 3. Simulated SSH snapshots (cm) on (left) 5 Jul 2000 and (right) 6 Jul 2006, with (a),(b) the original field, (c),(d) the MWT low-pass filtered components (decadal), (e),(f) the bandpass filtered components (interannual), and (g),(h) the high-pass filtered components (transient eddies).

the east (Figs. 4c,d). The IAPE and EAPE exhibit similar horizontal structures as IKE and EKE (Figs. 5b,c).

Compared to other energy components, the MAPE shows a different meridional distribution: minimum values are found along the axis of the jet, while it grows gradually both to the south and north side of the jet, with maximum value located at its adjacent recirculation gyre areas (Fig. 5a). This MAPE pattern seems counterintuitive at first glance, since most of the APE should be stored in the sloping KE jet rather than in its recirculation gyres

where isopycnal surfaces are observed mostly flat. Since APE is related to the perturbation density rather than the total density [see Eq. (10)] with a spatially constant reference density $\overline{\rho}(z)$ subtracted, it is not impossible that the MAPE has a minimum along the jet and maxima in the jet's recirculation gyres. But this is not essential. In fact, it is the released MAPE (MAPE change) rather than the MAPE itself that matters. Indeed, all the energetic terms in this study that account for the APE change are essentially confined to the jet.
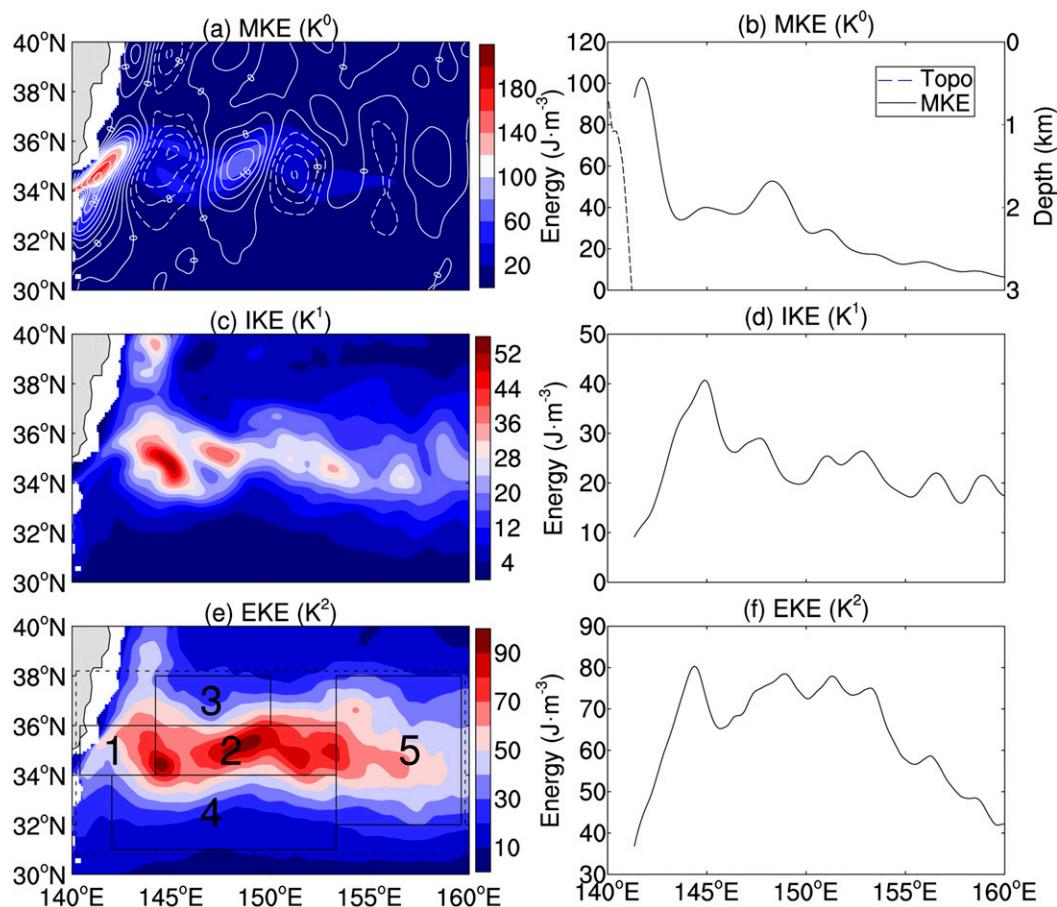
FIG. 4. Temporally and vertically (upper 1000 m) averaged multiscale KE components (J m^{-3}). (a) The horizontal structure of MKE and vertically averaged meridional velocity (solid lines; contour interval: 4 cm s^{-1}), and (b) the longitudinal distribution of MKE (solid) and bottom topography (dashed) meridionally averaged between 33° and 37°N. (c),(d) As in (a) and (b), but for IKE. (e),(f) As in (a) and (b), but for EKE. The labeled boxes in (e) mark the subdomains mentioned in the text.

To see the vertical structures of the multiscale energy components, a zonal–vertical sectional distribution is presented in Fig. 6. In general, all the three KE components are surface trapped (Figs. 6a–c). The wavelike amplitudes in KE fields drop remarkably with depth within the upper 500 m, indicating a surface-trapped mode in the vertical. The MKE show significant western intensification with their maximum values lying along the continental shelf (Fig. 6a). The interannual and transient eddy parts of KE do not peak until ~400 km downstream of the topography and spread more eastward than the low-frequency component (Figs. 6b,c). The APE components extend much deeper in the vertical (Figs. 6e–g), which exhibit interior maxima around ~400 m. Regarding the interannual and transient eddy components of APE (Figs. 6f,g), obvious surface intensification is observed within the surface layer. The vertical sections of IAPE and EAPE also exhibit

interior secondary maxima in the deep layers. Estimating from Argo floats, Roullet et al. (2014) also reported subsurface EAPE maxima in the Kuroshio Extension region, though the maximum depth is deeper than that in our results.

We have two observations about the above results. First, in terms of energy, the interannual-scale window is a reservoir comparable to the other two windows. Second, the Kuroshio Extension region from 140° to 160°E may be divided into a number of subdomains, that is, the nearshore eddy growth region west of 144°E, the eddy development region between 144° and 154°E, the eddy decaying region east of 154°E, as well as the NRG and SRG regions, which are marked and labeled by numbers in Fig. 4e. The vertical distributions of the area-mean energy densities are shown in Fig. 7. On the whole (Fig. 7a), the EKE is the largest reservoir among the three KE components, decaying rapidly with depth. By
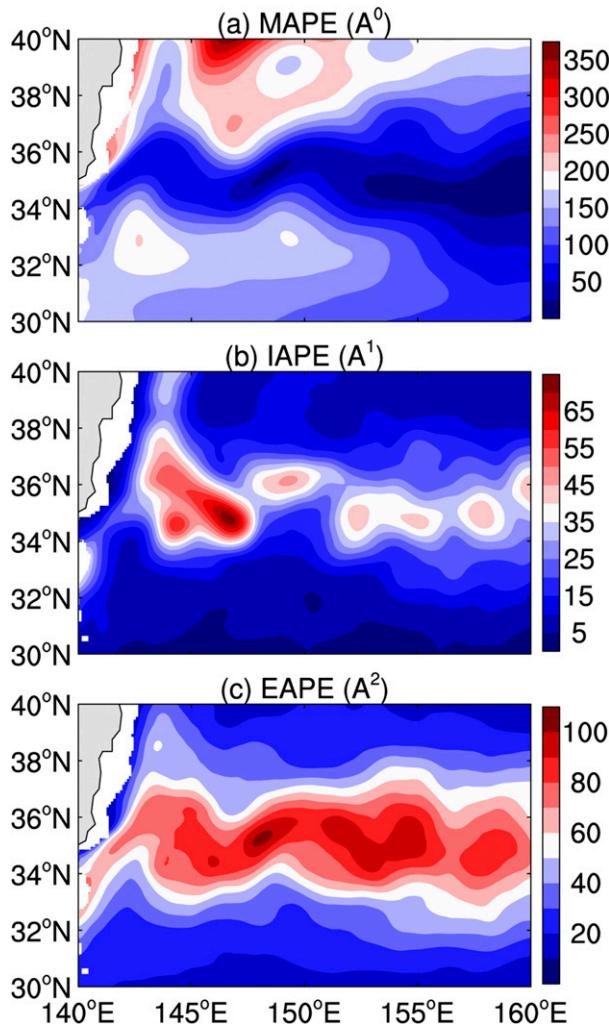
FIG. 5. As in the left column of Fig. 4, but for the multiscale APE components.

comparison, the MKE and IKE show much smaller magnitudes. This observation is consistent with previous studies such as Ferrari and Wunsch (2009), von Storch et al. (2012), and Scharffenberg and Stammer (2010). The KE also has a clear spatial variation. In the nearshore region (Fig. 7b), MKE > EKE > IKE in magnitude. Downstream from the nearshore region (Figs. 7c,f), the MKE decays drastically, while the IKE switches its position from the smallest to the second largest in some areas, such as the NRG, SRG, and the eddy decaying regions. Different from its KE counterpart, the relative proportion of the APE presents a clear dependence on depth. The relative magnitude of MAPE, IAPE, and EAPE shows a complex competition in the upper 200 m for all subdomains. In the deeper layers, the APE reservoirs from the largest to the smallest are MAPE, EAPE, and IAPE; their relative magnitudes are not

sensitive with the chosen subdomain, except in the eddy development region, where EAPE dominates (Fig. 7c). In the recirculation regions (Figs. 7d,e), it is evident that the MAPE is about one order larger in magnitude than others, consistent with Fig. 5a.

6. Multiscale interactions

An application of MS-EVA gives feature-rich energetic structures that allow us to gain insight into the complex dynamics of the Kuroshio Extension. In this section, we examine the time-mean spatial structure of the multiscale interactions (including the energy transfers and buoyancy conversions) in the related region. Based on a three-window decomposition, the MS-EVA enables us to further reveal the relative contribution of the mean–eddy, interannual–eddy, and mean–interannual interactions. Figure 8 shows the depth-averaged MS-EVA energetics maps. A general observation about Fig. 8 is that all energy terms are confined mainly along the jet, with strong values occupied just off the Japan coast. Another observation is that these terms present a clear along-stream variation: high and low centers usually appear one after another along the jet axis.

a. Mean–eddy interaction

The mean–eddy interaction terms from the EKE and EAPE budget equations are first analyzed. Figures 8e and 8g show the horizontal maps of vertically averaged barotropic $T_K^{0 \to 2}$ and baroclinic $T_A^{0 \to 2}$ transfers. Both $T_K^{0 \to 2}$ and $T_A^{0 \to 2}$ are positive and strong in the nearshore region, indicating that barotropic and baroclinic energy transfers from the mean flow are major energy sources of eddy growth in this region. Particularly, the large positive pool of $T_K^{0 \to 2}$ immediately downstream of the coastal topography corresponds well to the maximum MKE in Fig. 4a. This suggests that kinetic energy is first stored in the large-scale window and then is released to the transient eddies through barotropic instability. Additionally, the $T_A^{0 \to 2}$ field exhibits a cross-shore variation along the Japan Trench north of 36°N, where negative values are found on the inshore side of the trench and positive values are seen along the trench. Itoh and Yasuda (2010) reported dense areas of mesoscale eddies occur along the trench, while the eddy activity is much reduced on the inshore side of the trench. Our result demonstrates that the elevated baroclinicity along the trench contribute to the intense eddy activity at this area, whereas the flow on the inshore side of the trench are in fact baroclinically stable.

In contrast to the concentration of large positive energy transfer west of 145°E, the barotropic and baroclinic energy transfers exhibit positive and negative
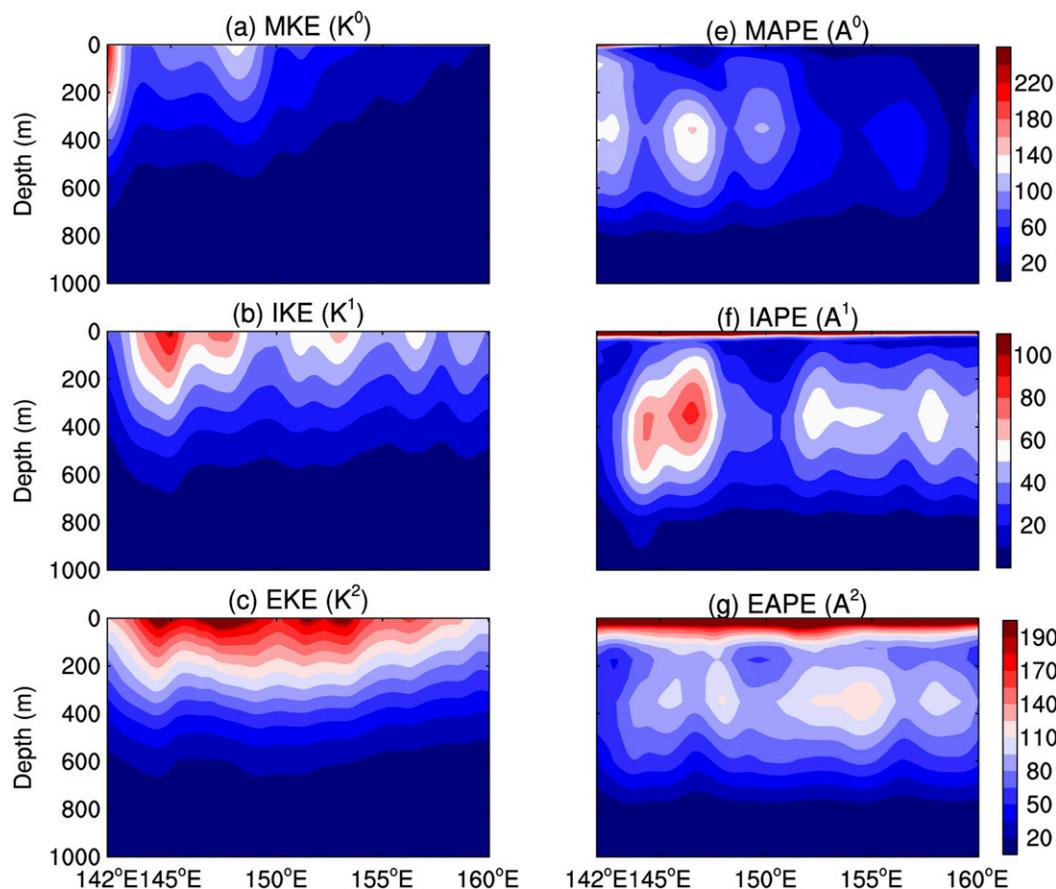
FIG. 6. Zonal–vertical sectional distributions of the multiscale energy components (J m^{-3}) averaged between 34° and 36°N. The left column shows (a) MKE, (b) IKE, and (c) EKE; the right column shows (d) MAPE, (e) IAPE, and (f) EAPE.

centers from 144° to 154°E. Overall, positive values of $T_K^{0 \to 2}$ are mainly confined around the jet axis, while negative values are observed at the northern and southern boundaries of the jet. Particularly, the upscale energy transfers are dominant in the places where NRG and SRG locate. Farther downstream from 154°E where the eddies are decaying, the EKE is mostly transferred to MKE, implying that eddies act to drive the mean circulation at this area. The horizontal pattern of $T_A^{0 \to 2}$ seems more patchy than $T_K^{0 \to 2}$ downstream from 144°E. On average, the mean flow loses energy in the eddy growing region and gains energy in the eddy decaying region.

The above analyses show a complex horizontal structure of the mean–eddy interaction in the Kuroshio Extension region. For the along-stream direction, the eddies tend to extract energy from the mean flow in the upstream regions, while they act to drive the mean flow downstream of the Kuroshio Extension. A number of previous studies have reported a similar mean–eddy interaction pattern in this region (Hall 1991; Waterman

et al. 2011; Chen et al. 2014). For the cross-stream direction, we find that the eddies generally act to drive the mean recirculation at its flanking recirculation regions. Some previous studies also reported the eddies' active role in strengthening the jet's flanking recirculations (Qiu et al. 2008; Taguchi et al. 2010; Delman et al. 2015).

The vertical structure of the energetics allows us to see the extent of the dynamic processes in the water column. Figure 9 shows the zonal–vertical section averaged between 34° and 36°N. The barotropic transfer displays a well-defined vertical structure that decays rapidly with depth (Fig. 9a). For the baroclinic transfer (Fig. 9d), it varies and even changes sign with depth, with deep maxima lying at 300–400 m. There is a good collocation between dEKE/dx and $T_K^{0 \to 2}$ in the zonal–vertical section. The positive $T_K^{0 \to 2}$ corresponds to the EKE growth region west of 144°E, while the negative $T_K^{0 \to 2}$ corresponds to the EKE decaying region east of 154°E. This indicates the barotropic stability/instability is the major mechanism for the EKE distribution in the related
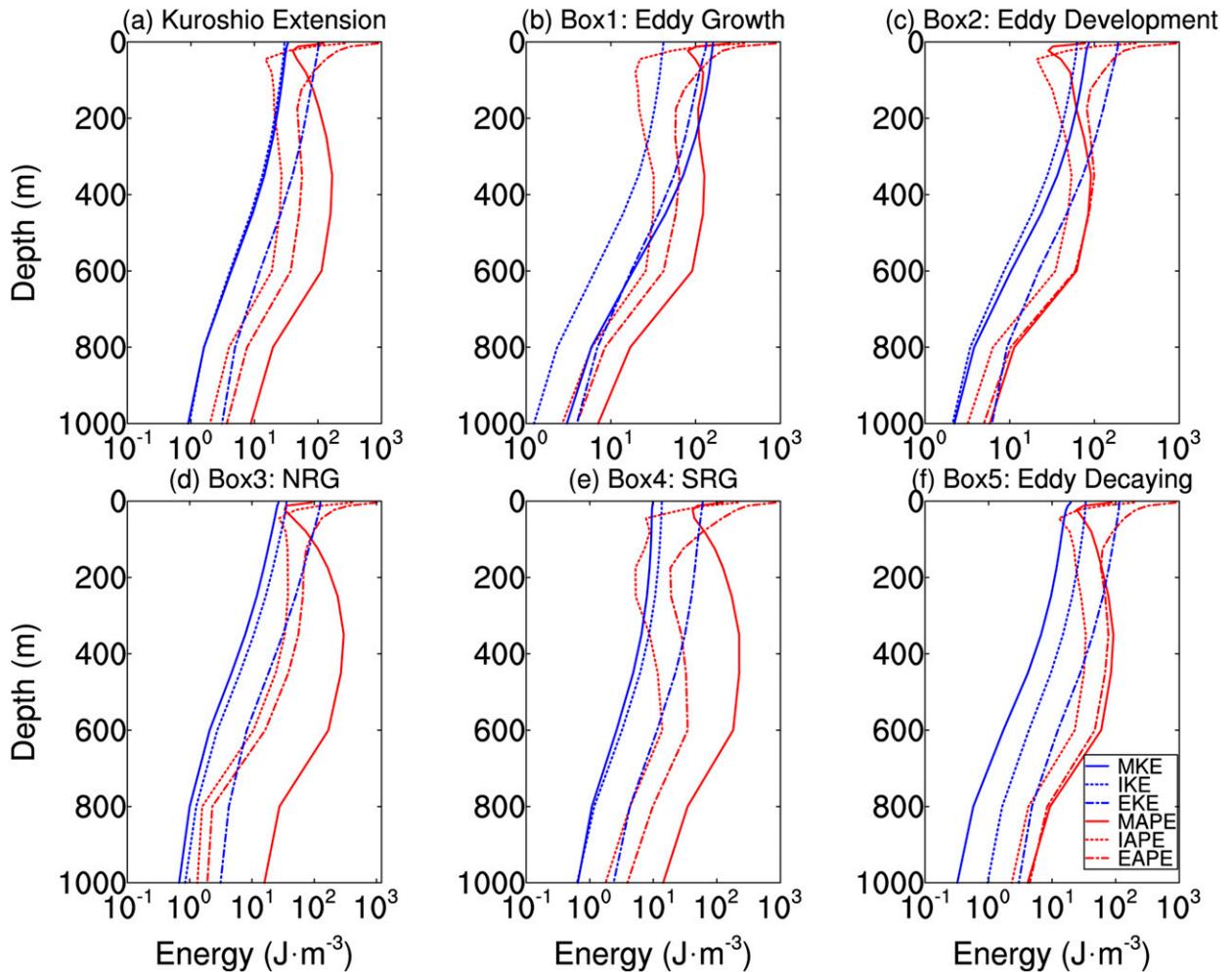
FIG. 7. The vertical distribution of the time-mean multiscale energy components (J m^{-3}) averaged over (a) the entire Kuroshio Extension region and (b)–(f) the five subdomains as marked in Fig. 4e.

region. To further illustrate the spatial variation of the energetics in the Kuroshio Extension region, Fig. 10 displays the vertical distribution of the area-mean energetics for all subdomains. The basic feature of $T_K^{0\rightarrow2}$ and $T_A^{0\rightarrow2}$ in the nearshore region is both terms are about one order of magnitude larger than those in other subdomains (Fig. 10b). The energy transferred from the mean to the eddy through barotropic and baroclinic instabilities is still an important factor for the downstream development of eddy disturbances (Fig. 10c), though we do not exclude other nonlocal mechanisms such as wave propagation. Researches along this line have been well documented in the literature both in oceanic and atmospheric storm tracks (Simmons and Hoskins 1978; Orlanski and Chang 1993; Williams et al. 2007; Chapman et al. 2015). In the east eddy decaying region, upscale energy transfer from EKE to MKE is significant, which indicates that the eddies act to drive

the mean flow in this region (Fig. 10f). Similar energy transfer direction is also observed for the baroclinic transfer below 200 m. Interestingly, the mean–eddy interaction of the two flanking recirculation subdomains resembles that of the eddy decaying region. For completeness, Fig. 8 also shows the horizontal maps of $T_K^{2\rightarrow0}$ and $T_A^{2\rightarrow0}$, these two terms are almost in opposite sign of $T_K^{0\rightarrow2}$ and $T_A^{0\rightarrow2}$, respectively, which demonstrates the localized feature of multiscale interactions (Liang and Robinson 2007).

b. Interannual–eddy interaction

The interaction analysis in MS-EVA enables us to further investigate the relative contribution between the mean–eddy and interannual–eddy interactions for the eddy dynamics in the Kuroshio Extension region. Overall, the interannual–eddy interaction is weaker than the mean–eddy interaction. Different from $T_K^{0\rightarrow2}$
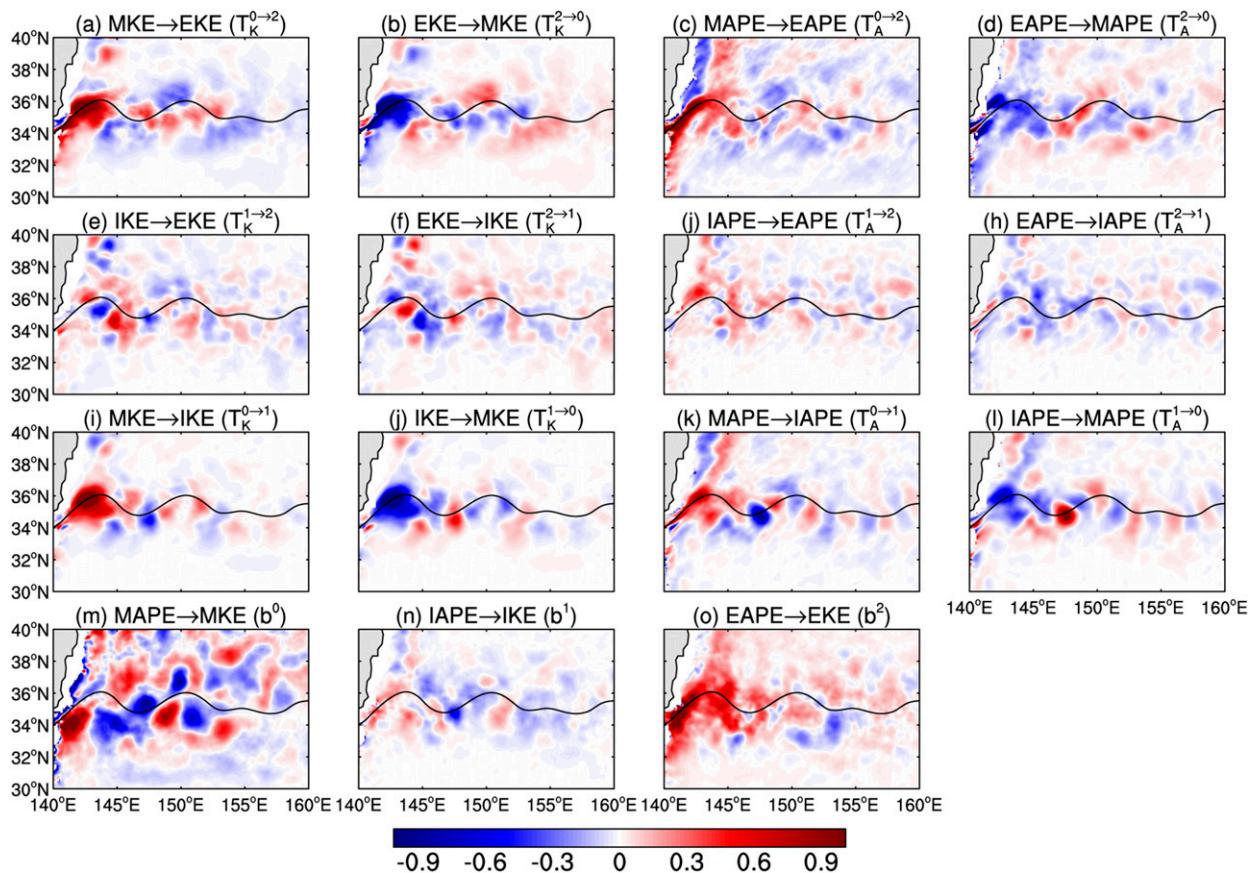
FIG. 8. Horizontal distributions of the time- and depth-averaged multiscale energetics (10^{-4} W m^{-3}). Superposed is the 50-cm contour of the SSH, which gives the jet axis.

and $T_A^{0\to2}$, $T_K^{1\to2}$ and $T_A^{1\to2}$ do not show a prominent positive center at the nearshore region (Figs. 8e,j and 9b,e), indicating that the energy provided for the eddy growth in this region mainly comes from the mean flow rather than from the interannual time scale. The spatial variation of the interannual–eddy interaction is better revealed in Fig. 10. In the nearshore region, the baroclinic $T_A^{1\to2}$ and barotropic transfers $T_K^{1\to2}$ are relatively weak; in fact, the eddies even transfer kinetic energy to the interannual scale (Fig. 10b). In the eddy development region, significant barotropic and baroclinic transfers from the interannual scale to the transient eddies are found. These positive energy transfers act as important energy sources to maintain the eddy development from 144° to 154°E. A number of previous studies, for instance, Chapman et al. (2015), reported that the storm track develops downstream from the initial baroclinic growth region through the ageostrophic flux of Montgomery potential. In this study, we find that the interannual time-scale energy is another source for the eddy development in this region. In the eddy decaying region (Fig. 10f), the eddies are found to

provide kinetic energy to the interannual-scale window. However, the term $T_A^{1\to2}$ does not show similar spatial variation as $T_K^{1\to2}$; it exhibits positive values for all subdomains, which means IAPE is always an important energy source for EAPE, which is then converted to EKE. The interannual–eddy interaction shows different directions in the two recirculation regions. On average, the eddies lose kinetic energy to the interannual time scale in the NRG region, while they gain kinetic energy at the SRG region.

c. Mean–interannual interaction

The interaction analysis further provides information for the mean–interannual interaction. So far, we have not learned of any reports on this type of scale interaction. A possible reason is that the interannual variability is disguised in the eddy window in a Reynolds time mean–eddy decomposition. In the nearshore region, the horizontal distribution of the mean–interannual interaction resembles that of the mean–eddy interaction, which implies that the decadally modulating mean flow loses kinetic energy to interannual scale as well as to the
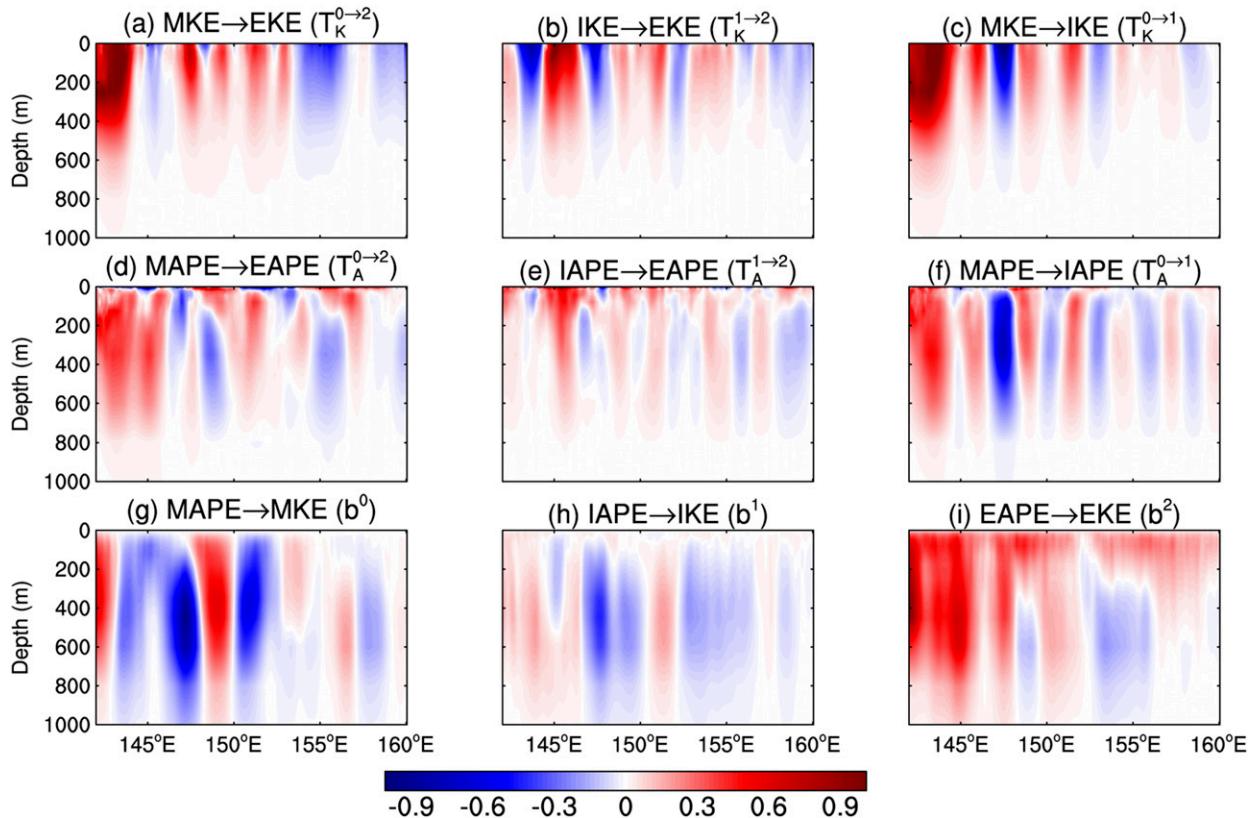
FIG. 9. Zonal–vertical distribution of the time-mean multiscale energetics (10^{-4} W m^{-3}) averaged between 34°–36°N.

transient eddies (Figs. 8i,k). In the downstream from 145°E, wavelike positive and negative centers of $T_K^{0 \to 1}$ and $T_A^{0 \to 1}$ are trapped along the jet axis. This feature indicates the interaction between the jet and jet-trapped Rossby waves, which is consistent with Sasaki et al. (2013) that the westward-propagating long Rossby waves in the Kuroshio Extension region travel along the sharp potential vorticity front of the jet with a narrow meridional scale and increasing amplitudes, rather than just propagate along a constant latitude. In a domain-averaged point of view, the vertical distributions of the area-mean $T_K^{0 \to 1}$ and $T_A^{0 \to 1}$ show positive values in the nearshore region, while the other subdomains exhibit complex mean–interannual interaction for both barotropic and baroclinic transfers (Fig. 10). For instance, the mean flow loses (gains) energy to (from) the interannual time scale for the barotropic (baroclinic) transfer in the eddy development region as well as the eddy decaying region, while the mean flow extracts energy from the interannual scale for both $T_K^{0 \to 1}$ and $T_A^{0 \to 1}$ in the SRG region.

d. Buoyancy conversion

Buoyancy conversion connects KE and APE on each individual window. In the vertical, the buoyancy conversion

extends rather deep through the water column (Figs. 9g–i). Among its three components, the b^0 field displays a relatively complex horizontal variation, which exhibits a clear along-stream as well as cross-stream variation (Fig. 8m). The b^1 field indicates the IKE converts energy to IAPE at most of locations in the Kuroshio Extension region, except for the nearshore place and a small region around 152°E (Figs. 8n, 9h). The b^2 field is found to be mostly positive in the entire region, indicating that a strong EAPE-to-EKE conversion occurs (Fig. 8o). In other words, the baroclinic eddy conversion is another major source of EKE growth in the Kuroshio Extension region. South of the jet axis between 150° to 155°E, there are negative centers in the b^2 field. These negative centers are not observed in the surface layers (Figs. 9i, 10f), indicating that in these deep areas the EAPE reservoir receives energy from the EKE reservoir. Several recent studies have suggested a similar feature in the ocean simulations, such as Zhai and Marshall (2013) and Kang and Curchitser (2015), which needs to be verified in the observation.

e. Energy pathway

To end this section, the energetics are schematized for the five subdomains and the entire region (Fig. 11). For
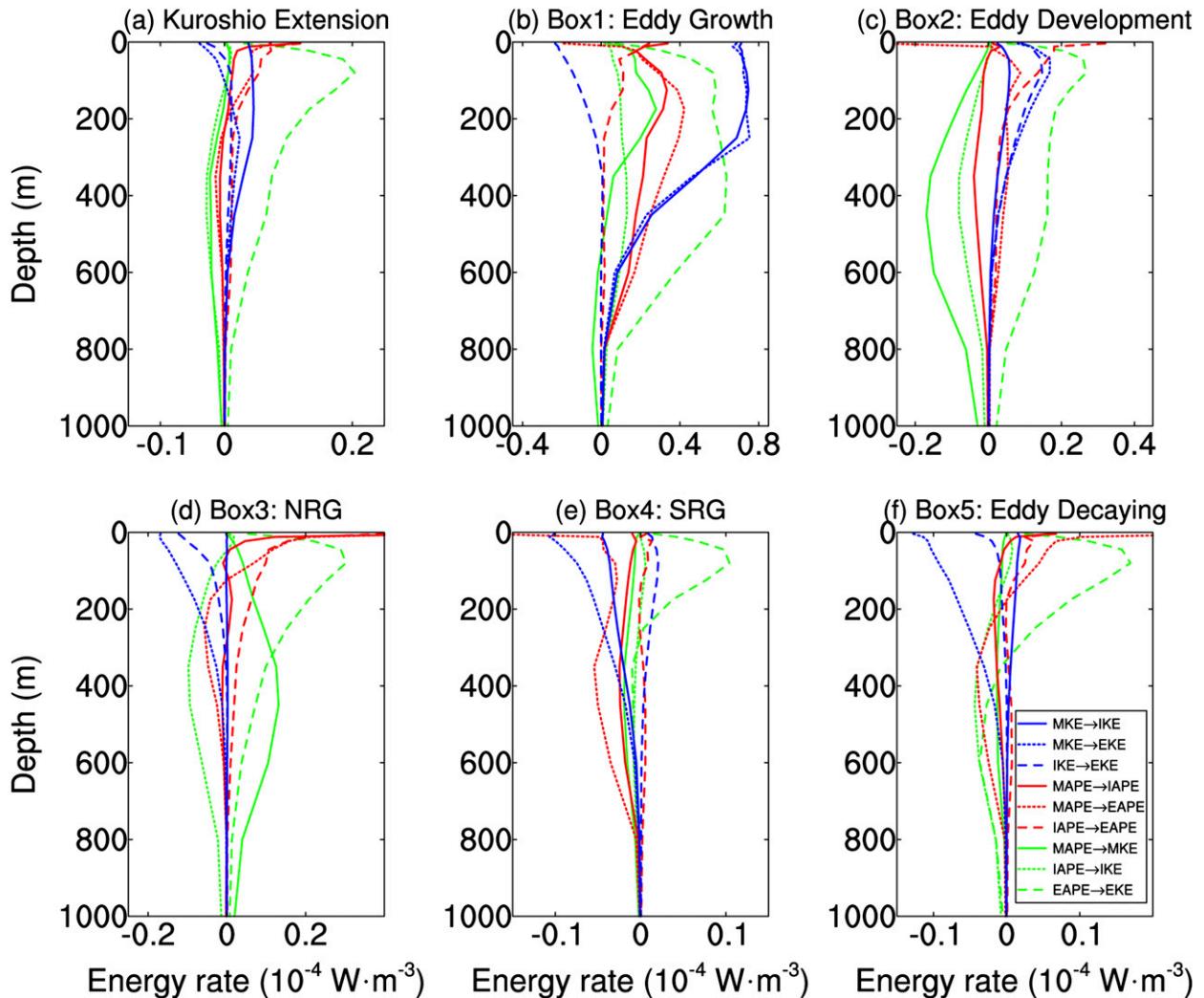
FIG. 10. The vertical distribution of the time-mean multiscale energetics (10^{-4} W m^{-3}) averaged over (a) the entire Kuroshio Extension region and (b)–(f) the five subdomains as indicated in Fig. 4e.

the entire Kuroshio Extension domain, roughly 40% of the energy released from the MKE reservoir is used to support the eddy growth, while the remaining 60% of kinetic energy is transferred to the interannual time scale. Apart from directly drawing energy from MKE, EKE also receives a great portion of energy from EAPE through buoyancy conversion. For the baroclinic transfers, about 80% of the energy released from the MAPE is used to sustain EAPE through baroclinic instability; at the same time, the EAPE draws a significant portion of energy from the IAPE reservoir. Beyond transferring kinetic energy to smaller scales, the MKE and IKE also convert energy to their APE counterparts to support the baroclinic eddy growth via inverse buoyancy conversion. The energy pathway in the nearshore area of eddy growth is analogous to that of the whole domain. This

is a region where strong localized barotropic and baroclinic transfers from the mean flow to the eddies are observed. In the eddy development subdomain, where anomalously high eddy energy is noted, evident energy transfer from the mean flow to the eddies, together with the transfer from the interannual time scale to the eddies, has been observed. For the NRG and SRG regions, the mean circulation draws energy not only from the eddies but also from the interannual variabilities to maintain itself. The interannual–eddy interaction exhibits different directions in the two regions. On average, the eddies lose kinetic energy to the interannual variability in the NRG region, while gaining kinetic energy in the SRG region. The eddy decaying subdomain is also characterized by a clear upscale energy transfer from the eddies to the mean flow. In this sense,
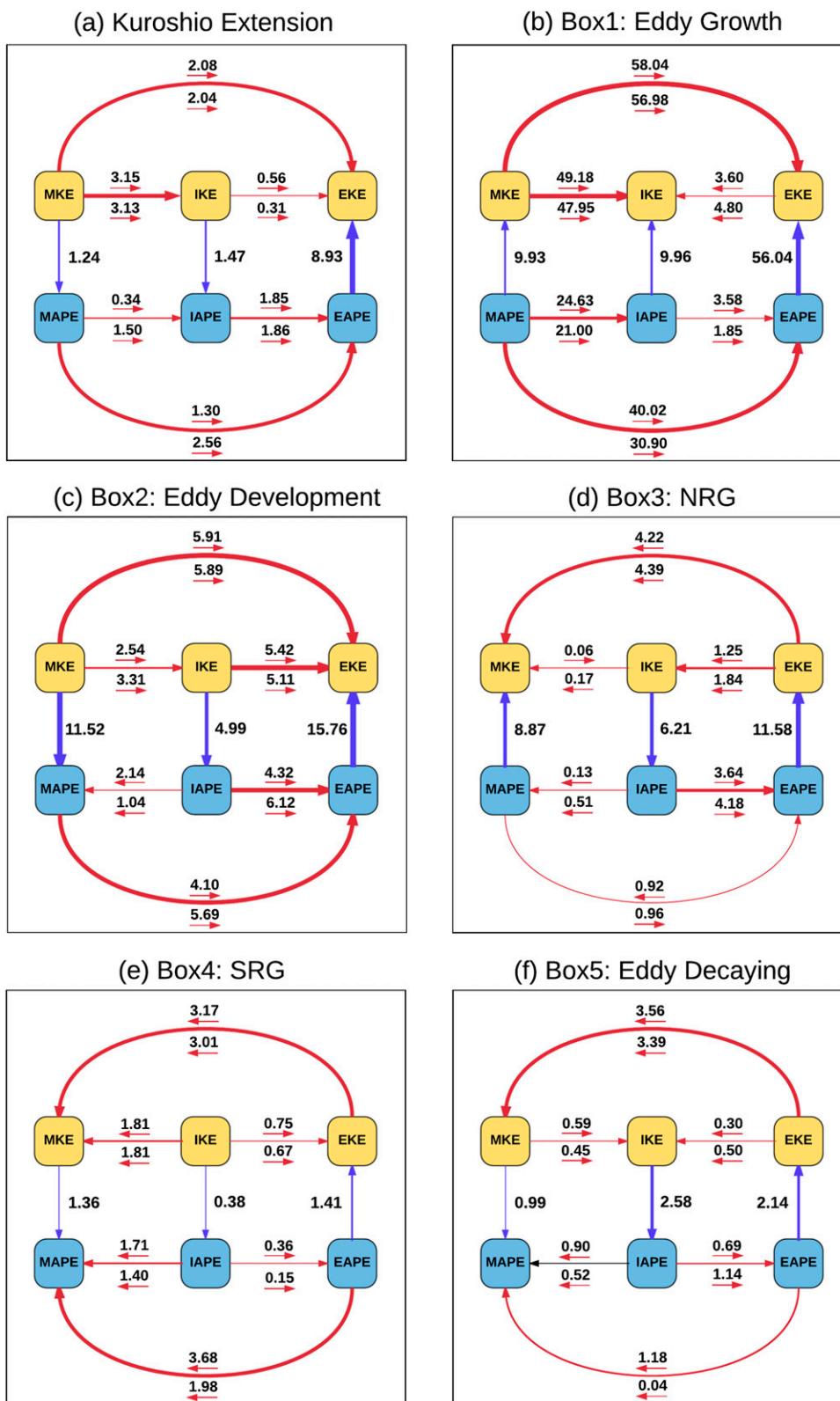
FIG. 11. Schematics of the volume-averaged energy pathway (as in Fig. 2) for (a) the entire Kuroshio Extension region and (b)–(f) the five subdomains as indicated in Fig. 4e. The multiscale energetics are in $10^{-6}\,\mathrm{W\,m^{-3}}$. A short arrow stands for the energy flow direction embedded in the energy transfers, and a long arrow stands for the overall energy flow direction between two different energy reservoirs.

our results confirmed the energy pathway in the Kuroshio Extension region, that is, the eddies act to decelerate the mean flow in the upstream of the region, whereas they act to accelerate the mean flow downstream of this region.

7. Summary and conclusions

The Kuroshio Extension system is rich in multiscale variabilities, including decadal modulation, interannual fluctuation, and transient mesoscale eddies (Mizuno and White 1983; Ebuchi and Hanawa 2000; Qiu and Chen 2005). Using the outputs from an eddy-resolving multidecadal hindcast simulation, a new energetics diagnostic tool (MS-EVA; Liang and Robinson 2005, 2007) was employed to investigate the climatological characteristics of these multiscale interactions. Instead of separating the original fields into a time mean and its deviation (Hall 1991; Qiu 1995; Waterman et al. 2011), or just separating the eddy fields through a temporal high-pass filter (Williams et al. 2007; Chapman et al. 2015), in this study, we used a new functional analysis tool (MWT; Liang and Anderson 2007) to decompose the original fields into three, orthogonal, separated parts (each in a scale window): the decadal modulating mean flow, the interannual fluctuation, and the transient eddies. This approach enables us to reveal the complex dynamics of mean–eddy, interannual–eddy, as well as mean–interannual interactions in the Kuroshio Extension region.

First examined are the multiscale energy components, which exhibit inhomogeneous spatial distributions. Specifically,

- the MKE maximizes immediately downstream of the Izu–Ogasawara Ridge; it follows the core of the stationary meander and decays dramatically downstream;
- the transient EKE does not peak until 400 km downstream of the ridge and remains anomalously high eastward until 154°E; and
- the interannual variability, which is dominated by a jet-trapped Rossby wave mode (Lin et al. 2014), is an energy reservoir comparable to those on the other two windows.

More importantly, we have explored the nonlinear interactions among the different scale windows. As above, the interactions also exhibit a distinct spatial pattern:

- In the nearshore eddy growth region, strong positive barotropic and baroclinic energy transfers from the mean flow to the eddies are observed immediately downstream of the ridge, while energy transfer from the interannual scale to the transient eddies are not significant in this region. The unstable mean jet also releases substantial energy to the interannual scale.
- In the eddy development region between 144° and 154°E, the energy transferred from the mean window to the eddy window, and that from the interannual window to the eddy window, are the two important factors for the development of the eddy disturbances.
- In the eddy decaying region east of 154°E, eddies act to drive the mean flow both for KE and APE fields. Regarding the interannual–eddy interaction, the eddies are found to provide KE to the interannual-scale window, while they extract APE from the interannual-scale window, which is further converted to EKE through buoyancy conversion. Interestingly, sequences of positive–negative centers are found along the mean jet axis in the map of mean-to-interannual interaction, with magnitudes increasing from east to west, indicating the interaction between the mean jet and jet-trapped long Rossby waves as observed by Sasaki and Schneider (2011).
- For the NRG and SRG regions, the mean flow draws energy not only from the eddies, but also from the interannual variabilities to maintain itself. The interannual–eddy interaction exhibits different directions in the two regions. On average, the eddies lose kinetic energy to the interannual variability in the NRG region, while gaining kinetic energy in the SRG region.

REFERENCES

Adamec, D., 1998: Modulation of the seasonal signal of the Kuroshio Extension during 1994 from satellite data. *J. Geophys. Res.*, **103**, 10 209–10 222, doi:10.1029/98JC00456.

Aoki, K., S. Minobe, Y. Tanimoto, and Y. Sasai, 2013: Southward eddy heat transport occurring along southern flanks of the Kuroshio Extension and the Gulf Stream in a 1/10° global ocean general circulation model. *J. Phys. Oceanogr.*, **43**, 1899–1910, doi:10.1175/JPO-D-12-0223.1.

Arbic, B. K., M. Müller, J. G. Richman, J. F. Shriver, A. J. Morten, R. B. Scott, G. Sérazin, and T. Penduff, 2014: Geostrophic

turbulence in the frequency–wavenumber domain: Eddy-driven low-frequency variability. *J. Phys. Oceanogr.*, **44**, 2050–2069, doi:10.1175/JPO-D-13-054.1.

Bernstein, R. L., and W. B. White, 1981: Stationary and traveling mesoscale perturbations in the Kuroshio Extension current. *J. Phys. Oceanogr.*, **11**, 692–704, doi:10.1175/1520-0485(1981)011<0692:SATMPI>2.0.CO;2.

Bishop, S. P., 2013: Divergent eddy heat fluxes in the Kuroshio Extension at 144°–148°E. Part II: Spatiotemporal variability. *J. Phys. Oceanogr.*, **43**, 2416–2431, doi:10.1175/JPO-D-13-061.1.

Brooks, I. H., and P. P. Niiler, 1977: Energetics of the Florida Current. *J. Mar. Res.*, **35**, 163–191.

Chapman, C. C., A. M. Hogg, A. E. Kiss, and S. R. Rintoul, 2015: The dynamics of Southern Ocean storm tracks. *J. Phys. Oceanogr.*, **45**, 884–903, doi:10.1175/JPO-D-14-0075.1.

Chen, R., G. R. Flierl, and C. Wunsch, 2014: A description of local and nonlocal eddy–mean flow interaction in a global eddy-permitting state estimate. *J. Phys. Oceanogr.*, **44**, 2336–2352, doi:10.1175/JPO-D-14-0009.1.

Delman, A. S., J. L. McClean, J. Sprintall, L. D. Talley, E. Yulaeva, and S. R. Jayne, 2015: Effects of eddy vorticity forcing on the mean state of the Kuroshio Extension. *J. Phys. Oceanogr.*, **45**, 1356–1375, doi:10.1175/JPO-D-13-0259.1.

Ebuchi, N., and K. Hanawa, 2000: Mesoscale eddies observed by TOLEX-ADCP and TOPEX/POSEIDON altimeter in the Kuroshio recirculation region south of Japan. *J. Oceanogr.*, **56**, 43–57, doi:10.1023/A:1011110507628.

——, and ——, 2001: Trajectory of mesoscale eddies in the Kuroshio recirculation region. *J. Oceanogr.*, **57**, 471–480, doi:10.1023/A:1021293822277.

Ferrari, R., and C. Wunsch, 2009: Ocean circulation kinetic energy: Reservoirs, sources, and sinks. *Annu. Rev. Fluid Mech.*, **41**, 253–282, doi:10.1146/annurev.fluid.40.111406.102139.

Gill, A. E., 1982: *Atmosphere–Ocean Dynamics.* Academic Press, 662 pp.

Greatbatch, R. J., X. Zhai, J.-D. Kohlmann, and L. Czeschel, 2010: Ocean eddy momentum fluxes at the latitudes of the Gulf Stream and the Kuroshio Extensions as revealed by satellite data. *Ocean Dyn.*, **60**, 617–628, doi:10.1007/s10236-010-0282-6.

Hall, M. M., 1991: Energetics of the Kuroshio Extension at 35°N, 152°E. *J. Phys. Oceanogr.*, **21**, 958–975, doi:10.1175/1520-0485(1991)021<0958:EOTKEA>2.0.CO;2.

Hurlburt, H. E., A. J. Wallcraft, W. J. Schmitz, P. J. Hogan, and E. J. Metzger, 1996: Dynamics of the Kuroshio/Oyashio Current System using eddy-resolving models of the North Pacific Ocean. *J. Geophys. Res.*, **101**, 941–976, doi:10.1029/95JC01674.

Itoh, S., and I. Yasuda, 2010: Characteristics of mesoscale eddies in the Kuroshio–Oyashio Extension region detected from the distribution of the sea surface height anomaly. *J. Phys. Oceanogr.*, **40**, 1018–1034, doi:10.1175/2009JPO4265.1.

Jayne, S. R., and Coauthors, 2009: The Kuroshio Extension and its recirculation gyres. *Deep Sea Res.*, **56**, 2088–2099, doi:10.1016/j.dsr.2009.08.006.

Joyce, T. M., 1987: Hydrographic sections across the Kuroshio Extension at 165°E and 175°W. *Deep Sea Res.*, **34**, 1331–1352, doi:10.1016/0198-0149(87)90130-0.

Kang, D., and E. N. Curchitser, 2015: Energetics of eddy–mean flow interactions in the Gulf Stream region. *J. Phys. Oceanogr.*, **45**, 1103–1120, doi:10.1175/JPO-D-14-0200.1.

Kelly, K. A., L. Thompson, W. Cheng, and E. J. Metzger, 2007: Evaluation of HYCOM in the Kuroshio Extension region using new metrics. *J. Geophys. Res.*, **112**, C01004, doi:10.1029/2006JE002678.

Liang, X. S., and A. R. Robinson, 2004: A study of the Iceland–Faeroe frontal variability using the multiscale energy and vorticity analysis. *J. Phys. Oceanogr.*, **34**, 2571–2591, doi:10.1175/JPO2661.1.

——, and ——, 2005: Localized multiscale energy and vorticity analysis: I. Fundamentals. *Dyn. Atmos. Oceans*, **38**, 195–230, doi:10.1016/j.dynatmoce.2004.12.004.

——, and D. G. M. Anderson, 2007: Multiscale window transform. *Multiscale Model. Simul.*, **6**, 437–467, doi:10.1137/06066895X.

——, and A. R. Robinson, 2007: Localized multi-scale energy and vorticity analysis: II. Finite-amplitude instability theory and validation. *Dyn. Atmos. Oceans*, **44**, 51–76, doi:10.1016/j.dynatmoce.2007.04.001.

——, and ——, 2009: Multiscale processes and nonlinear dynamics of the circulation and upwelling events off Monterey Bay. *J. Phys. Oceanogr.*, **39**, 290–313, doi:10.1175/2008JPO3950.1.

Lin, H., K. R. Thompson, and J. Hu, 2014: A frequency-dependent description of propagating sea level signals in the Kuroshio Extension region. *J. Phys. Oceanogr.*, **44**, 1614–1635, doi:10.1175/JPO-D-13-0185.1.

Masumoto, Y., and Coauthors, 2004: A fifty-year eddy-resolving simulation of the World Ocean: Preliminary outcomes of OFES (OGCM for the Earth Simulator). *J. Earth Simul.*, **1**, 35–56.

McCalpin, J. D., and D. B. Haidvogel, 1996: Phenomenology of the low-frequency variability in a reduced-gravity, quasigeostrophic double-gyre model. *J. Phys. Oceanogr.*, **26**, 739–752, doi:10.1175/1520-0485(1996)026<0739:POTLFV>2.0.CO;2.

Mizuno, K., and W. B. White, 1983: Annual and interannual variability in the Kuroshio Current System. *J. Phys. Oceanogr.*, **13**, 1847–1867, doi:10.1175/1520-0485(1983)013<1847:AAIVIT>2.0.CO;2.

Nakamura, H., and A. S. Kazmin, 2003: Decadal changes in the North Pacific oceanic frontal zones as revealed in ship and satellite observations. *J. Geophys. Res.*, **108**, 3078, doi:10.1029/1999JC000085.

Nonaka, M., H. Nakamura, Y. Tanimoto, T. Kagimoto, and H. Sasaki, 2006: Decadal variability in the Kuroshio–Oyashio Extension simulated in an eddy-resolving OGCM. *J. Climate*, **19**, 1970–1989, doi:10.1175/JCLI3793.1.

——, ——, ——, ——, and ——, 2008: Interannual-to-decadal variability in the Oyashio and its influence on temperature in the subarctic frontal zone: An eddy-resolving OGCM simulation. *J. Climate*, **21**, 6283–6303, doi:10.1175/2008JCLI2294.1.

——, H. Sasaki, B. Taguchi, and H. Nakamura, 2012: Potential predictability of interannual variability in the Kuroshio Extension jet speed in an eddy-resolving OGCM. *J. Climate*, **25**, 3645–3652, doi:10.1175/JCLI-D-11-00641.1.

Orlanski, I., and E. K. M. Chang, 1993: Ageostrophic geopotential fluxes in downstream and upstream development of baroclinic waves. *J. Atmos. Sci.*, **50**, 212–225, doi:10.1175/1520-0469(1993)050<0212:AGFIDA>2.0.CO;2.

Pacanowski, R. C., and S. M. Griffies, 1999: The MOM3 manual. NOAA/Geophysical Fluid Dynamics Laboratory Ocean Group Tech. Rep. 4, 680 pp.

Pedlosky, J., 1987: *Geophysical Fluid Dynamics.* 2nd ed. Springer-Verlag, 710 pp.

Penduff, T., M. Juza, B. Barnier, J. Zika, W. K. Dewar, A.-M. Treguier, J.-M. Molines, and N. Audiffren, 2011: Sea level expression of intrinsic and forced ocean variabilities at interannual time scales. *J. Climate*, **24**, 5652–5670, doi:10.1175/JCLI-D-11-00077.1.

Qiu, B., 1995: Variability and energetics of the Kuroshio Extension and its recirculation gyre from the first two-year TOPEX data. *J. Phys. Oceanogr.*, **25**, 1827–1842, doi:10.1175/1520-0485(1995)025<1827:VAEOTK>2.0.CO;2.

——, 2000: Interannual variability of the Kuroshio Extension system and its impact on the wintertime SST field. *J. Phys. Oceanogr.*, **30**, 1486–1502, doi:10.1175/1520-0485(2000)030<1486:IVOTKE>2.0.CO;2.

——, and S. Chen, 2005: Variability of the Kuroshio Extension jet, recirculation gyre, and mesoscale eddies on decadal time scales. *J. Phys. Oceanogr.*, **35**, 2090–2103, doi:10.1175/JPO2807.1.

——, and ——, 2010: Eddy-mean flow interaction in the decadally modulating Kuroshio Extension system. *Deep-Sea Res. II*, **57**, 1098–1110, doi:10.1016/j.dsr2.2008.11.036.

——, K. A. Kelly, and T. M. Joyce, 1991: Mean flow and variability in the Kuroshio Extension from Geosat altimetry data. *J. Geophys. Res.*, **96**, 18 491–18 507, doi:10.1029/91JC01834.

——, S. Chen, P. Hacker, N. G. Hogg, S. R. Jayne, and H. Sasaki, 2008: The Kuroshio Extension northern recirculation gyre: Profiling float measurements and forcing mechanism. *J. Phys. Oceanogr.*, **38**, 1764–1779, doi:10.1175/2008JPO3921.1.

Roullet, G., X. Capet, and G. Maze, 2014: Global interior eddy available potential energy diagnosed from Argo floats. *Geophys. Res. Lett.*, **41**, 1651–1656, doi:10.1002/2013GL059004.

Sasaki, H., M. Nonaka, Y. Masumoto, Y. Sasai, H. Uehara, and H. Sakuma, 2008: An eddy-resolving hindcast simulation of the quasiglobal ocean from 1950 to 2003 on the Earth Simulator. *High Resolution Numerical Modelling of the Atmosphere and Ocean*, K. Hamilton and W. Ohfuchi, Eds., Springer, 157–185, doi:10.1007/978-0-387-49791-4_10.

Sasaki, Y. N., and N. Schneider, 2011: Decadal shifts of the Kuroshio Extension jet: Application of thin-jet theory. *J. Phys. Oceanogr.*, **41**, 979–993.

——, S. Minobe, and N. Schneider, 2013: Decadal response of the Kuroshio Extension jet to Rossby waves: Observation and thin-jet theory. *J. Phys. Oceanogr.*, **43**, 442–456, doi:10.1175/JPO-D-12-096.1.

Scharffenberg, M. G., and D. Stammer, 2010: Seasonal variations of the large-scale geostrophic flow field and eddy kinetic energy inferred from the TOPEX/Poseidon and *Jason-1* tandem mission data. *J. Geophys. Res.*, **115**, C02008, doi:10.1029/2008JC005242.

Simmons, A. J., and B. J. Hoskins, 1978: The life cycles of some nonlinear baroclinic waves. *J. Atmos. Sci.*, **35**, 414–432, doi:10.1175/1520-0469(1978)035<0414:TLCOSN>2.0.CO;2.

Spall, M. A., 1996: Dynamics of the Gulf Stream/deep western boundary current crossover. Part II: Low-frequency internal oscillations. *J. Phys. Oceanogr.*, **26**, 2169–2182, doi:10.1175/1520-0485(1996)026<2169:DOTGSW>2.0.CO;2.

——, 2000: Generation of strong mesoscale eddies by weak ocean gyres. *J. Mar. Res.*, **58**, 97–116, doi:10.1357/002224000321511214.

Taguchi, B., S.-P. Xie, N. Schneider, M. Nonaka, H. Sasaki, and Y. Sasai, 2007: Decadal variability of the Kuroshio Extension: Observations and an eddy-resolving model hindcast. *J. Climate*, **20**, 2357–2377, doi:10.1175/JCLI4142.1.

——, B. Qiu, M. Nonaka, H. Sasaki, S.-P. Xie, and N. Schneider, 2010: Decadal variability of the Kuroshio Extension: Mesoscale eddies and recirculations. *Ocean Dyn.*, **60**, 673–691, doi:10.1007/s10236-010-0295-1.

Tai, C.-K., and P. P. Niiler, 1985: Modeling large-scale instabilities in the Kuroshio Extension. *Dyn. Atmos. Oceans*, **9**, 359–382, doi:10.1016/0377-0265(85)90009-0.

——, and W. B. White, 1990: Eddy variability in the Kuroshio Extension as revealed by Geosat altimetry: Energy propagation away from the jet, Reynolds stress, and seasonal cycle. *J. Phys. Oceanogr.*, **20**, 1761–1777, doi:10.1175/1520-0485(1990)020<1761:EVITKE>2.0.CO;2.

Tracey, K. L., D. R. Watts, K. A. Donohue, and H. Ichikawa, 2012: Propagation of Kuroshio Extension meanders between 143° and 149°E. *J. Phys. Oceanogr.*, **42**, 581–601, doi:10.1175/JPO-D-11-0138.1.

von Storch, J.-S., C. Eden, I. Fast, H. Haak, D. Hernández-Deckers, E. Maier-Reimer, J. Marotzke, and D. Stammer, 2012: An estimate of the Lorenz energy cycle for the World Ocean based on the STORM/NCEP simulation. *J. Phys. Oceanogr.*, **42**, 2185–2205, doi:10.1175/JPO-D-12-079.1.

Waterman, S., N. G. Hogg, and S. R. Jayne, 2011: Eddy–mean flow interaction in the Kuroshio Extension region. *J. Phys. Oceanogr.*, **41**, 1182–1208, doi:10.1175/2010JPO4564.1.

Williams, R. G., C. Wilson, and C. W. Hughes, 2007: Ocean and atmosphere storm tracks: The role of eddy vorticity forcing. *J. Phys. Oceanogr.*, **37**, 2267–2289, doi:10.1175/JPO3120.1.

Wyrtki, K., L. Magaard, and J. Hager, 1976: Eddy energy in the oceans. *J. Geophys. Res.*, **81**, 2641–2646, doi:10.1029/JC081i015p02641.

Xie, L., X. Liu, and L. J. Pietrafesa, 2007: Effect of bathymetric curvature on Gulf Stream instability in the vicinity of the Charleston Bump. *J. Phys. Oceanogr.*, **37**, 452–475, doi:10.1175/JPO2995.1.

Yamagata, T., Y. Shibao, and S. Umatanit, 1985: Interannual variability of the Kuroshio Extension and its relation to the Southern Oscillation/El Niño. *J. Oceanogr. Soc. Japan*, **41**, 274–281, doi:10.1007/BF02109276.

Zhai, X., and D. P. Marshall, 2013: Vertical eddy energy fluxes in the North Atlantic Subtropical and Subpolar Gyres. *J. Phys. Oceanogr.*, **43**, 95–103, doi:10.1175/JPO-D-12-021.1.